J. Fluid Mech. (2006), *vol.* 569, *pp.* 349–363.
doi:10.1017/S0022112006002886 Printed in the United Kingdom

Hysteresis and non-uniqueness in the speed of the onset of instability in curtain coating

By J. O. MARSTON[1,2], S. P. DECENT[1] AND M. J. H. SIMMONS[2]

[1]School of Mathematics, The University of Birmingham, Edgbaston, Birmingham, B15 2TT, UK

[2]Department of Chemical Engineering, The University of Birmingham, Edgbaston, Birmingham, B15 2TT, UK

(Received 13 February 2006 and in revised form 12 June 2006)

The maximum speed of stable coating is determined experimentally by the onset of air entrainment in curtain coating onto a pre-wetted surface over a broad range of dimensionless parameters (Reynolds number: $0.14 < Re < 33.02$; capillary number: $0.19 < Ca < 25.07$). We show not only that the substrate speed at the onset of instability is flow-rate dependent for a pre-wetted surface, but that the speed at which instability occurs is not always unique for a given flow rate.

1. Introduction

Blake & Ruschak (1979) described a maximum speed of stable wetting in experimental observations of an advancing contact line across a dry solid surface. Below this speed of wetting, the contact line, where the solid–liquid interface intersects the liquid–gas interface, advances in a stable manner and the uniform coating of the liquid onto the solid substrate is possible. Once this speed is passed, the wetting line was observed to become unstable and air entrainment was observed to occur at the wetting line. It has generally been thought that the speed at which the wetting line becomes unstable for given parameters is unique, i.e. below this maximum speed the wetting line is always stable, and above it, the wetting line is always unstable. Once unstable, the wetting line will normally adopt a 'sawtooth' configuration and air is entrained between the liquid and the solid at the vertices of the 'teeth'. Many previous studies have determined contact line speeds at the onset of air entrainment for coating onto a dry smooth surface (Burley & Kennedy 1976; Blake & Ruschak 1979; Gutoff & Kendrick 1982; Burley & Jolly 1984; Ghannam & Esmail 1993; Blake, Clarke & Ruschak 1994; Cohu & Benkreira 1998; Blake, Bracke & Shikhmurzaev 1999; Benkreira 2002; Blake & Shikhmurzaev 2002), and found the speed at the onset of instability to be unique for a given set of flow conditions. The maximum substrate speed at the onset of air entrainment is generally shown to be inversely proportional to the fluid viscosity. These studies were performed by holding all experimental parameters constant and increasing the substrate speed to determine the onset of the instability.

However, under certain situations it is possible to demonstrate non-uniqueness. Clarke (2002) showed the existence of multiple stable regions for the curtain coating of Newtonian fluids onto a rough surface, whilst Blake, Dobson & Ruschak (2004) noted a similar effect on smooth surfaces using a greatly increased curtain height.

Coating flows have been reviewed recently by Weinstein & Ruschak (2004) and the advances in modelling of dynamic wetting have been reviewed by Blake (2005).

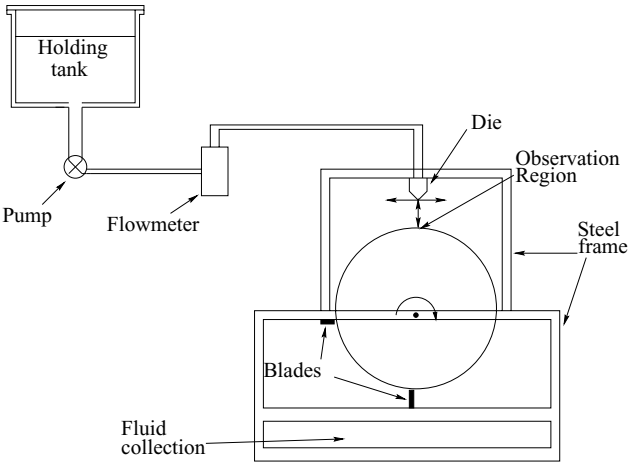

FIGURE 1. Schematic of the curtain coating apparatus used.

For a concise review of some of the experimental and theoretical correlations for air entrainment data see Benkreira (2004).

This paper describes a series of curtain coating experiments, for a related but different problem, where the substrate is pre-wetted with a thin film of the coating fluid. These experiments show that the speed at the onset of instability is, in some cases, not unique for a given set of flow conditions. When this is the case, the results show that the speed at which the contact line becomes unstable is determined by the path taken through the flow rate–substrate speed parameter space. The experimental method utilized here is different to that employed in the experimental papers listed above, since the route through this parameter space is varied. It is found that, at certain points in the parameter space, it is possible to observe either stable coating or air entrainment (i.e. unstable coating). That is, hysteresis is observed in the parameter space.

2. Experimental setup and method

A schematic of the curtain coating facility is shown in figure 1. The continuous substrate was provided by a rotating stainless steel wheel, with a diameter of 0.45 m and a width of 0.06 m. The surface was highly polished so that the average surface deviation (R_a) was $52\,\text{nm} \pm 2\,\text{nm}$. The wheel was capable of producing various substrate speeds, U, with a maximum speed of $2.3\,\text{m}\,\text{s}^{-1}$. The fluids were supplied to a four-slot die of width 0.09 m using a high-accuracy gear pump and the flow rates, Q, were measured by an electromagnetic flow meter. The flow meter was calibrated by weighing collected fluid over certain time intervals and flow rates and determined to be accurate to within 3.5 %. The integrity of the falling curtain over the free-fall height, h, was maintained by using copper wires and Perspex windows as edge guides. The liquid falls from the die and coats the surface of the wheel. This film coating is partially removed on the underside of the wheel, to leave a smooth, very thin film on the surface of the wheel.

The fluids used were aqueous solutions of glycerol, producing solutions with viscosities μ ranging from 0.0326 to 0.878 Pa s, densities ρ from 1196 to $1270\,\text{kg}\,\text{m}^{-3}$, and surface tensions σ from 0.0642 to $0.0678\,\text{N}\,\text{m}^{-1}$ respectively. Thus the Reynolds

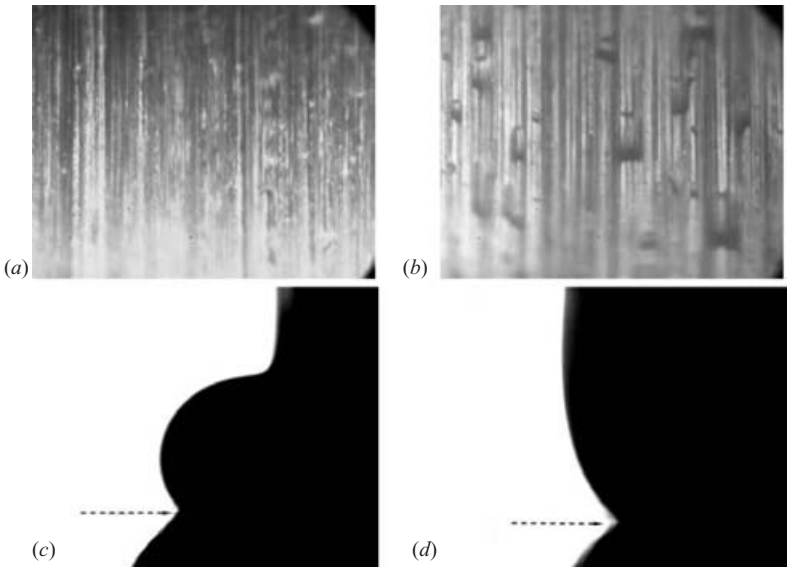

FIGURE 2. Images taken of (*a*) the pre-wetted wheel surface which forms the coating substrate as viewed from above for standard cleaning (squeegees), (*b*) the wheel surface as viewed from above with additional cleaning mechanisms of a water wash and air knife showing drops, (*c*) free surface profile for a 0.0326 Pa s solution for $h = 85$ mm, $U = 0.27\,\mathrm{m\,s^{-1}}$ and $Q = 2.44\,\mathrm{cm^2\,s^{-1}}$ and (*d*) free surface profile for a 0.245 Pa s solution for $h = 85$ mm, $U = 0.29\,\mathrm{m\,s^{-1}}$ and $Q = 2.34\,\mathrm{cm^2\,s^{-1}}$. Image (*c*) shows the 'heel' formation. The arrows in (*c*) and (*d*) lie in the plane of the liquid film substrate and point at the wetting line. Below the arrows reflection from the surface of the wheel can be seen.

number $0.14 < Re = \rho Q/\mu < 33.02$ and capillary number $0.16 < Ca = \mu U/\sigma < 25.07$ both spanned three orders of magnitude. The measurements of the physical properties were made at the ambient temperature of the laboratory, which remained constant for the duration of a single experiment. All fluids were mixed then left overnight to equilibrate with the laboratory temperature, which was confirmed by measurement. Static values of surface tension were determined using a du Nouy ring tensiometer; these values may differ appreciably from the dynamic value at the impingement zone (Lin & Roberts 1981).

Removal of the bulk of the liquid film from the solid substrate post-coating was performed using two double-v-headed urethane 'squeegee' blades. The blades were mounted between steel plates, bolted to the outer frame and pressed tightly against the surface. These blades remove most, but not all of the liquid, leaving a residual film. The coating surface was therefore pre-wetted and estimates of the thickness of the residual film were obtained by placing absorbent material onto the rotating wheel before the coating die for 10 revolutions during the coating process. Results for the thickness of the residual film indicate that it is at least of the order of 10^{-7} 10^{-6} m, sufficient to eliminate any surface roughness effects (Clarke 2002). Images of the surface of the wheel presented in figure 2 were taken using a 1280×1024 pixel CCD camera and image grabber attached to a personal computer. Image (*a*) shows the pre-wetted solid surface with the residual thin film, produced using the squeegee blade scrapers, onto which coating occurs. It can be seen that the film is smooth (the film itself cannot be seen). In comparison, the use of additional cleaning mechanisms (water wash and air knife) gives image (*b*), which shows, in this case, the surface

is clearly non-uniform with distinct drops. From the shapes of the drops, it can be seen that the surface topography has a strong influence on the wetting properties of the wheel. Thus, this additional cleaning was not done since this would lead to a highly non-uniform surface. It was checked in the experimental results presented here that the coating was always onto a smooth film (as in figure 2*a*), rather than onto a non-uniform film with drops (as in figure 2*b*). By altering the tension of the blades, it was possible to vary the thickness of the film. Although the thickness is marginally dependent upon viscosity and speed, repeatability of results implies that the film thickness does not vary dynamically throughout the experiments, hence the hysteresis is due to true nonlinear effects of the flow. The influence of the pre-wetted film thickness can be significant (Chen, Rame & Garoff 2004); however this influence is not the focus of the current work.

Side-on images of the free surface in the vicinity of the contact line were also taken and some example images of stable profiles are given in figure 2(*c*, *d*). Back illumination was provided by a 90 W fibre-optic light guide placed behind the rear of the curtain. Due to the limitations on the available resolution, it was decided not to study the contact angle evolution. Instead, side-on images and digital photographs were taken at various points through the Q–U parameter space to show both stable and unstable configurations.

Measurements of the wheel speed at the onset of air entrainment were made for a constant curtain height h of 95 mm. Although increasing the flow rate can lead to a slight increase in mean curtain velocity near the tip of the die, this effect is negligible for curtain heights greater than a few centimetres (Blake *et al.* 1994) and hence the impingement speed can be calculated as $u_i = \sqrt{2gh} \approx 1.36\,\mathrm{m\,s^{-1}}$ so that increasing Q leads to an increase in curtain width $w = Q/u_i$ (Blake *et al.* 2004).

The onset of air entrainment was obtained by slowly increasing the substrate (wheel) speed U at constant curtain flow rate Q until the liquid failed to coat the wheel surface and entrainment of air bubbles was observed with the naked eye. The substrate speed was then slowly reduced until the re-emergence of stability was observed (usually termed 'clearance'). In some cases, there was a notable difference between the speeds at the onset and clearance of air entrainment. This creates a region of hysteresis. In the hysteresis region, it can be considered that there are at least two competing attractors: one corresponding to stable coating without air entrainment, and the other corresponding to air entrainment.

In true dynamic wetting problems, dynamic wetting failure – where the wetting line ceases to advance normal to itself and adopts a sawtooth configuration – can occur before the onset of air entrainment. Equally, when the surface is pre-wetted, the liquid may fail to coat the surface before air entrainment occurs. However, these two points could not be distinguished in these experiments, hence instability is defined only by the onset of air entrainment in this paper. The procedure described above to generate the data points was repeated for a number of increasing values of curtain flow rates Q until the substrate speed at the onset of air entrainment was no longer a function of Q. Each data point was repeated at least three times and the observed variation in the speed at the onset of instability was less than 3 %.

This procedure can be viewed as the usual method of determining the speed of onset of instability, and is that adopted in previous experimental studies. This procedure was then varied by examining the instability boundary by moving through the Q–U parameter space in different ways. This included fixing U and increasing Q to examine changes in stability/instability. More elaborate paths through the parameter space were also examined.

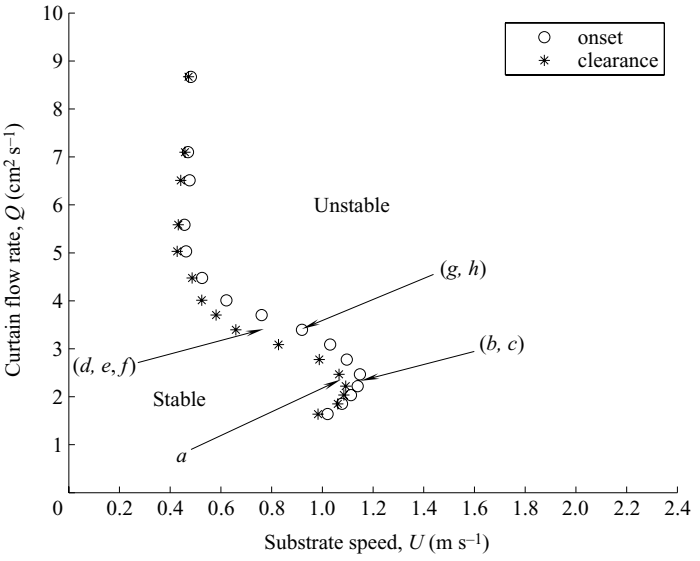

FIGURE 3. Air entrainment (onset–clearance) curves for an aqueous glycerol solution ($\mu = 0.119$ Pa s, $\sigma = 0.065$ N m^{-1}). The data points (circles and stars) were obtained by increasing and decreasing the substrate speed for fixed values of the curtain flow rate Q, and mark the onset and clearance of air entrainment respectively for fixed Q. The arrows point to the locations of both digital photographs and curtain profile images given in figure 4. $0.78 < Ca < 2.1$, $1.73 < Re < 9.15$.

3. Results and discussion

3.1. *Horizontal analysis of the Q–U parameter space*

An example of the usually defined window for stable curtain coating is given in figure 3 for a low-viscosity fluid ($\mu = 0.119$ Pa s). The data points shown as circles were obtained by setting the flow rate Q to a constant and then increasing the substrate speed U from well within the successful coating region (0.2 m s^{-1}) until instability occurred. The stars show clearance of air entrainment found by decreasing the substrate speed U for a constant flow rate Q until stable coating is again observed. If the substrate speed is increased from a stable configuration for a constant flow rate, the contact line will eventually become unstable and air will be entrained which is visible to the naked eye (onset). From this point, the instability will remain and air entrainment persists until the substrate speed is reduced sufficiently that air entrainment is no longer visible (clearance). This difference between onset and clearance of instability is air entrainment hysteresis. This hysteresis occurrence has been observed by Blake *et al.* (1994) for coating of non-Newtonian fluids onto dry substrates and by Kistler for a pre-wetted surface (see Miyamoto & Katagiri 1997). In comparison, no hysteresis is observed when coating onto a dry smooth surface for simple fluids (Blake *et al.* 1994). Hence the pre-wetted surface may be providing lubrication which causes the fluid to act in a non-Newtonian manner.

The arrows on figure 3 indicate the locations of images taken at the impingement zone of the curtain, which are presented in figure 4. Digital images are taken from either the front or rear of the curtain and profile (silhouette) images are taken from the side. Figures 4(*a*)–4(*c*) are taken at the value of Q for which the maximum substrate speed ($U = 1.14$ m s^{-1}) occurs. Figure 4(*a*) is taken at a stable configuration (clearance) and figures 4(*b*) and 4(*c*) are taken at the onset of air entrainment from

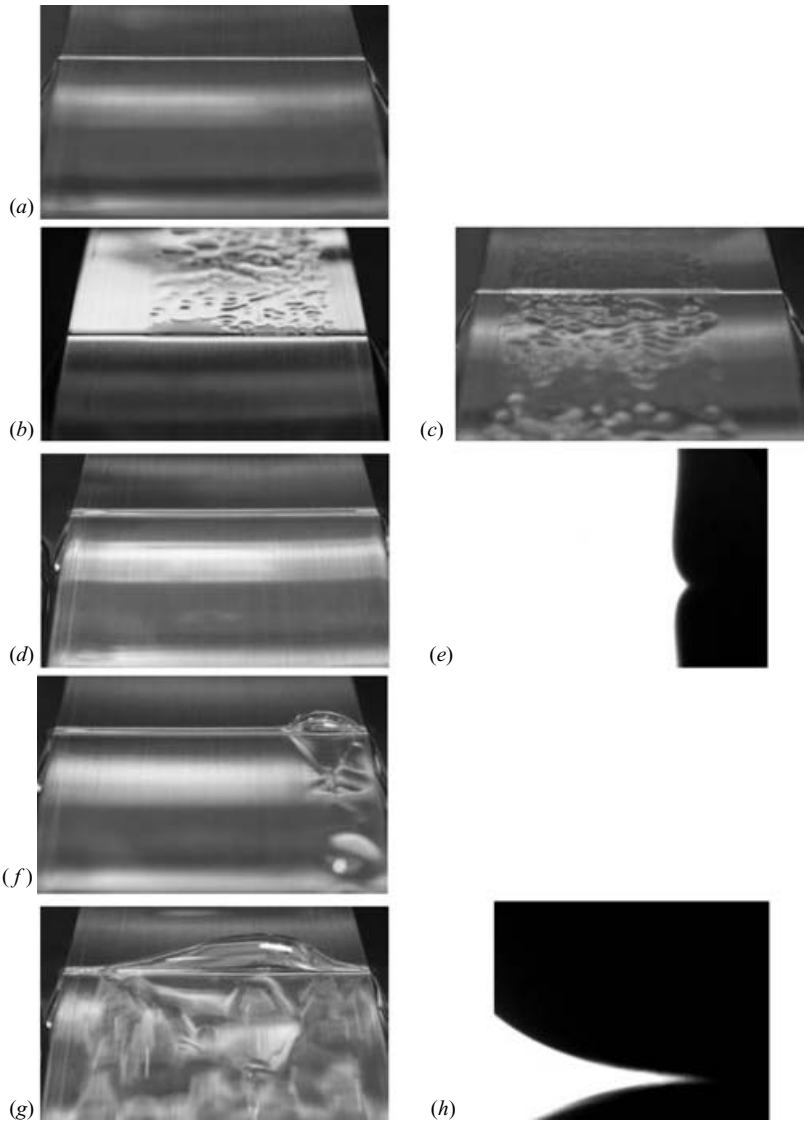

FIGURE 4. Digital photographs and curtain profile images corresponding to the locations marked on the air entrainment curve in figure 3. The parameters (Q, U) for each image are as follows: (a) (2.35, 1.04), (b, c) (2.35, 1.12), $(d–f)$ (3.39, 0.76), (g, h) (3.39, 0.92). Images (d) (produced by increasing speed from a stable configuration) and (f) (produced by reducing speed from an unstable configuration) show that the flow can be either stable or unstable for identical parameters in the hysteresis region.

the rear and front of the curtain respectively; the rippling of the film on the substrate is due to the entrained air.

Figures 4(d)–4(h) are taken at a higher flow rate $Q = 3.39\,\mathrm{cm^2\,s^{-1}}$. Figure 4$(d)$ shows stable coating and 4(e) is the corresponding side image of the back of the curtain. Figure 4(g) is the front elevation taken at the onset of air entrainment, which is accompanied by large heel formation to the rear of the curtain, the bottom of which is shown in figure 4(h). Figures 4(d) and 4(f) are taken at the same substrate speed in the hysteresis region. Figure 4(d) was taken during the production of the onset

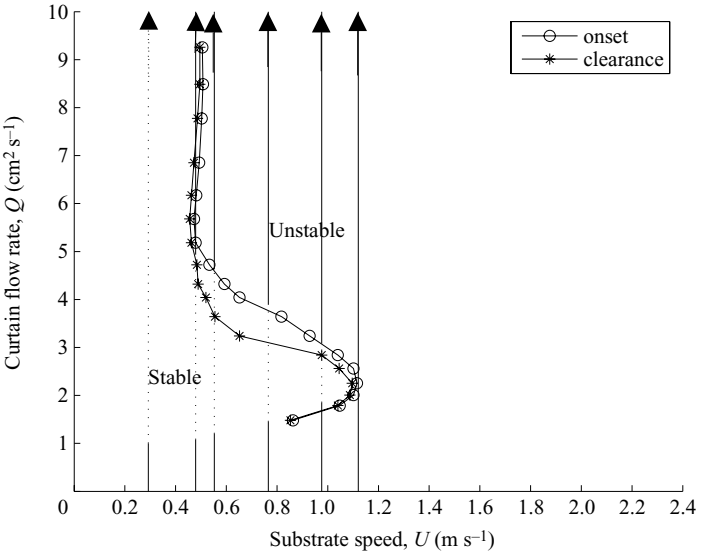

FIGURE 5. Air entrainment (onset–clearance) curves for an aqueous glycerol solution ($\mu = 0.124$ Pa s, $\sigma = 0.0664$ N m^{-1}). The data points (circles and stars) were obtained by increasing and decreasing the substrate speed for fixed values of the curtain flow rate Q, and mark the onset and clearance of air entrainment respectively for fixed Q. The stable coating window is reproduced for constant substrate speed (vertical lines) and increasing flow rate. The solid parts denote observations of air entrainment and the dotted parts represent successful coating with a stable contact line. $0.85 < Ca < 2.09$, $1.54 < Re < 9.65$.

curve in figure 3 and shows stable coating, whilst figure 4(f) was taken during the determination of the clearance of air entrainment, hence demonstrating the existence of multiple states at the same experimental parameters. Upon the re-emergence of stability, the contact line resumes its original position relative to the curtain.

Figure 5 shows air entrainment data for a fluid of a similar viscosity ($\mu = 0.124$ Pa s) to that in figure 3. A maximum substrate speed of 1.11 m s^{-1} for stable coating is reached at a flow rate of 2.25 cm^2 s^{-1} in figure 5. For flow rates $Q < 2.25$ cm^2 s^{-1}, there is little hysteresis effect (since the onset and clearance curves largely overlap), but for flow rates $Q > 2.25$ cm^2 s^{-1} there is a considerable difference between the onset and clearance, which creates the hysteresis region. For $Q > 5$ cm^2 s^{-1}, the onset of instability is no longer flow-rate dependent and the hysteresis becomes negligible once again. This onset curve defines a stable coating window, and is typical for a Newtonian fluid using the curtain coating method onto dry substrates (Blake *et al.* 1994, 1999). The heel formation, shown in figure 2(c), can occur in the stable region for low substrate speeds and moderate flow rates, and so in figure 5, this corresponds to the left of the clearance data points for $Q > 3$ cm^2 s^{-1}.

Figure 6 shows data points for the onset of instability for a 0.462 Pa s solution with two residual film thicknesses of $O(10^{-6}$ m) and $O(10^{-5}$ m) respectively. For the former, a smooth coating window as for low-viscosity fluids is no longer possible as there is a bifurcation of the stability curves at $Q = 5.31$ cm^2 s^{-1}, which is distinguished by the 'upper' and 'lower' branches, represented by open and filled circles respectively. The high coating speeds attained on the lower branch are attributed to 'intense' hydrodynamic assist (Blake *et al.* 2004), in which air entrainment can be postponed to significantly higher coating speeds by the variation of Q. Once the maximum

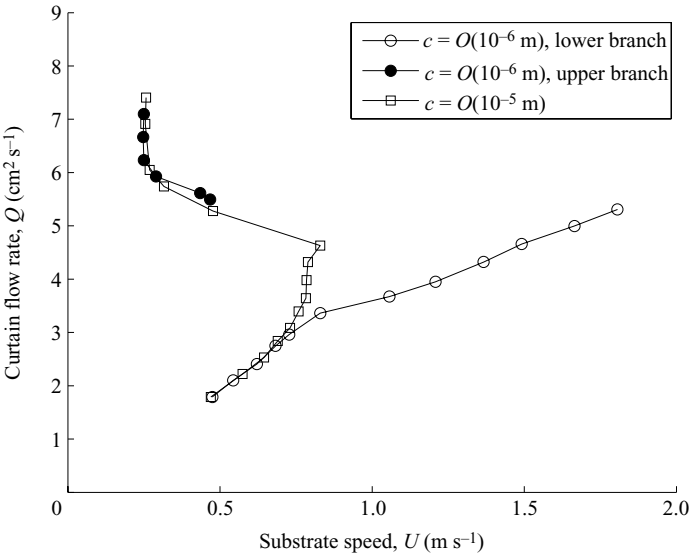

FIGURE 6. Air entrainment (onset) curves for increasing residual film thickness, c, for a 0.462 Pa s solution ($\sigma = 0.065\,\mathrm{N\,m^{-1}}$). By increasing the thickness approximately one order of magnitude, there is no longer a bifurcation and the data points fall onto one curve, that is the intense assist is lost. $1.77 < Ca < 12.86$, $0.49 < Re < 2.03$.

coating speed $U = 1.81\,\mathrm{m\,s^{-1}}$ is reached on the lower branch, any further increases in Q lead to a dramatic reduction in the onset speed (upper branch). By altering the tension of the blades against the wheel, it was possible to produce a residual film approximately an order of magnitude larger. The data points for the onset in this situation are also given in figure 6 (squares). The first few data points lie on the original lower branch, but depart from it at $Q = 3\,\mathrm{cm^2\,s^{-1}}$ to reach a maximum substrate speed $U = 0.83\,\mathrm{m\,s^{-1}}$, after which the onset speeds fall and rejoin the original upper branch. Since the intense assist and hence bifurcation of stability curves was not witnessed for a film thickness of this magnitude, the bifurcation for the residual film thickness of $O(10^{-6}\,\mathrm{m})$ was examined in the rest of this study. Clearly, under the conditions of intense assist, the inverse relationship between the substrate speed at the onset of air entrainment and the fluid viscosity no longer holds.

The data points in figure 7 (triangles/circles and stars) show the onset and clearance of air entrainment for a higher viscosity fluid (0.597 Pa s). Intense hydrodynamic assist is witnessed for flow rates $Q > 3\,\mathrm{cm^2\,s^{-1}}$, which gives a maximum speed of stable coating of $1.84\,\mathrm{m\,s^{-1}}$ at a flow rate of $5.98\,\mathrm{cm^2\,s^{-1}}$. Throughout this range of flow rates, the discrepancies between the upper and lower boundaries of air entrainment (i.e. the onset and clearance boundaries, shown by triangles and stars) become substantial, creating an enlarged region of hysteresis. For flow rates below this range ($Q < 3\,\mathrm{cm^2\,s^{-1}}$), the hysteresis effect is negligible. For flow rates above this range ($Q > 5.98\,\mathrm{cm^2\,s^{-1}}$), the maximum stable substrate speeds drop dramatically and converges to a limiting value of $0.27\,\mathrm{m\,s^{-1}}$, and the hysteresis effect becomes negligible once again.

3.2. *Vertical analysis of the Q–U parameter space*

The coating windows for the 0.124 and 0.597 Pa s fluids described above were re-examined by setting the substrate speed U at a constant value and increasing the

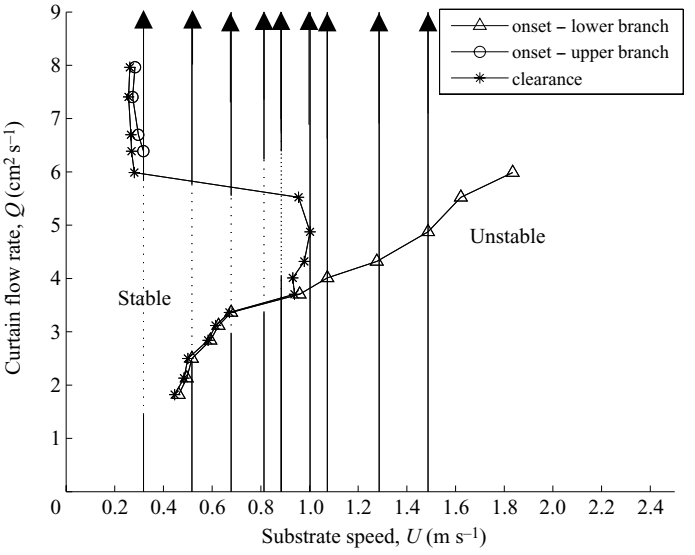

FIGURE 7. Air entrainment (onset–clearance) curves for an aqueous glycerol solution ($\mu = 0.597$ Pa s, $\sigma = 0.0647$ N m^{-1}). The data points were obtained by increasing (triangles and circles) and decreasing (stars) the substrate speed for fixed values of the curtain flow rate Q, and mark the onset and clearance of air entrainment respectively for fixed Q. The stable coating window is re-examined for constant substrate speed (vertical lines) and increasing flow rate. The solid parts denote observations of air entrainment and the dotted parts represent successful coating with a stable contact line. $2.39 < Ca < 16.93$, $0.386 < Re < 1.689$.

curtain flow rate Q. The results of this procedure are given in figures 5 and 7, and are examined in turn. The vertical lines represent measurements over a constant substrate speed U. The solid parts denote observations of air entrainment, and the dotted sections denote successful coating with a stable contact line. Clearly, if coating is started to the right of the onset curve in figure 5, air entrainment is always expected. This is verified by the far-right line for a constant speed of 1.12 m s^{-1} where air entrainment persisted for the entire range of flow rates. For a low substrate speed, represented by the far-left line, air entrainment was visible only at the lowest flow rate. As soon as this was increased, the contact line quickly became stable and no air entrainment was observed thereafter. For all the intermediate substrate speeds tested, the contact line was initially unstable and air entrainment was observed at low flow rates. The contact line stabilized with a small increase in flow rate and successful coating was achieved. It was then possible to increase the flow rate until the upper onset boundary (i.e. the onset curve shown by the circles, found by a horizontal examination of the Q–U parameter space) was reached. It can be seen that the stable coating window previously described was almost exactly reproducible using this alternative method.

The results of this procedure for the 0.597 Pa s solution are also shown by the vertical lines in figure 7. It can be seen that the lower boundary of the stable region defined for increasing flow rate (lower end of the dotted sections of the vertical lines) coincides to some extent with the equivalent boundary obtained for clearance by decreasing the substrate speed (clearance data points, shown by stars). For low substrate speeds corresponding to the three left-most vertical lines, the upper boundary of the stable region (top of the dotted section) coincides with the clearance boundary (i.e. stars)

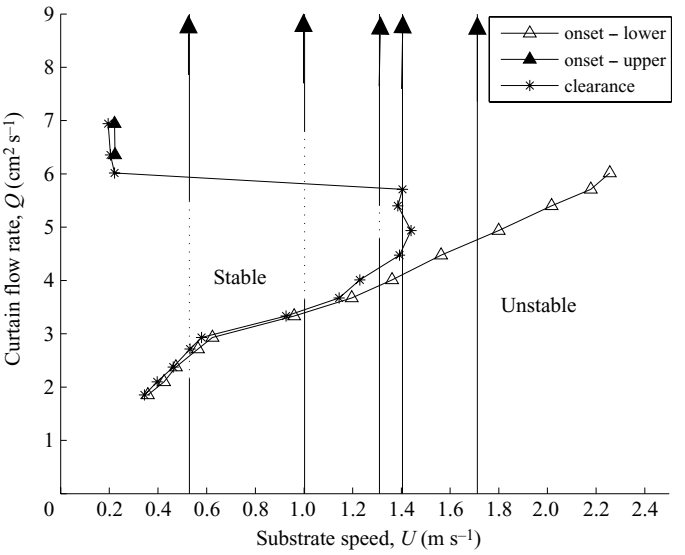

FIGURE 8. Air entrainment (onset–clearance) curves for an aqueous glycerol solution ($\mu = 0.552$ Pa s, $\sigma = 0.0648$ N m^{-1}). The data points were obtained by increasing (open and filled triangles) and decreasing (stars) the substrate speed for fixed values of the curtain flow rate Q, and mark the onset and clearance of air entrainment respectively for fixed Q. Data for a vertical examination at constant substrate speed (vertical lines) and increasing flow rate are also given. The solid parts denote observations of air entrainment and the dotted parts represent successful coating with a stable contact line.

of air entrainment. This indicates that, for low substrate speeds, it is not possible to maintain a stable contact line by passing through the apparent hysteresis region in this fashion. In comparison, for slightly higher substrate speeds (central two vertical lines) the contact line does remain stable through the hysteresis region and successful coating is achieved in the unstable region defined by the horizontal analysis. On passing through the hysteresis region from an unstable configuration for a constant substrate speed, stable coating is never reached: this can be seen from the four far-right vertical lines.

A vertical analysis was also performed for constant U but decreasing Q for another high-viscosity fluid where intense assist was known to occur. The differences between an increasing vertical analysis and a decreasing vertical analysis are presented in figures 8 and 9 respectively, where the arrows give the direction of variation in Q. The vertical lines in both figures are for the same values of U. As can be seen, the stability regions created using these vertical analyses are not the same. The contact line remains stable over a broader range of flow rates for increasing Q than for decreasing: this is seen from the left three vertical lines. In figure 9 the instability appears to persist well into the 'stable' region (defined from horizontal analysis) when decreasing Q (this is seen from all three lines where stability was detected), whereas stability can persist through the hysteresis and into the 'unstable' regions in figure 8.

3.3. *Path-dependent analysis of the Q–U parameter space*

From the data presented in figures 5 and 7, it can be deduced that stable coating in the hysteresis region will depend upon how points in that region are reached. That is to say if the hysteresis region is approached from a point of known stability (where there is no air entrainment), then stable coating is sometimes possible. If it is

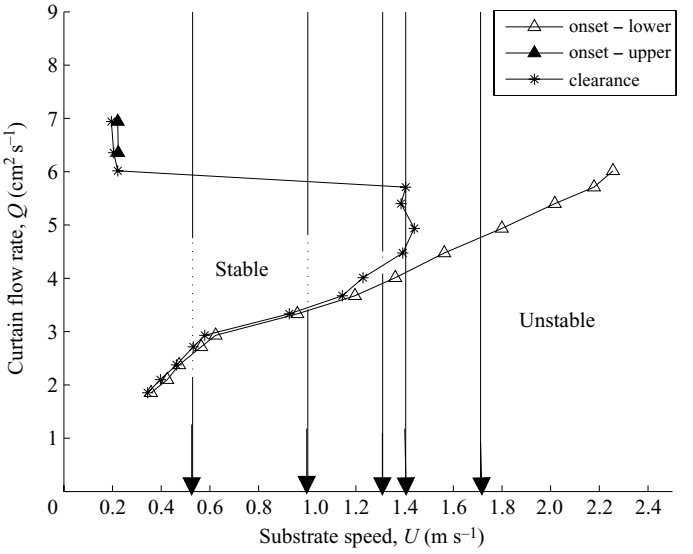

FIGURE 9. Air entrainment (onset–clearance) curves for an aqueous glycerol solution ($\mu = 0.552$ Pa s, $\sigma = 0.0648$ N m^{-1}). The data points are those from figure 8. Data for a vertical examination at constant substrate speed (vertical lines) and decreasing flow rate are also given. The solid parts denote observations of air entrainment and the dotted parts represent successful coating with a stable contact line. $1.62 < Ca < 19.16$, $0.42 < Re < 1.59$.

approached from a point of known instability (where air entrainment is occurring), then stable coating is not possible. That is, once instability occurs, it will persist inside the hysteresis region, as should be expected.

In view of this observation, the path taken to enter the hysteresis region for the high-viscosity fluid was altered. By starting from within the stable coating region and alternately increasing the substrate speed and flow rate, it was possible to achieve stability beyond the upper boundary (created by the data points for constant Q) observed in figure 7. The results for this procedure are presented in figure 10. There is an enlarged region of stability obtained by using this method. Therefore for $6.2\,\text{cm}^2\,\text{s}^{-1} < Q < 8\,\text{cm}^2\,\text{s}^{-1}$, it can be seen that there are at least two substrate speeds for the onset of air entrainment i.e. two distinct speeds at which the contact line becomes unstable, and the speed at the onset of instability will depend upon the path taken through the parameter space to reach that instability. The first of these two speeds is determined by increasing the substrate speed at a constant flow rate, and the second (greater speed) is determined by passing through the hysteresis region and alternately increasing both flow rate and substrate speed. This phenomenon is shown to also occur in figures 11 and 13, for different high-viscosity fluids (0.608 and 0.498 Pa s).

Figure 11 shows the two branches for the onset of instability (marked by circles joined by a solid line) for a horizontal analysis. The data points joined by the dotted line mark the onset of air entrainment from the path-dependent analysis. The filled circles indicate limitations of the equipment, i.e. the three far-right points are the maximum possible substrate speed and the top point is the limit of the pump. Hence, for this fluid, a closed region of stability could not be found. The letters (a–f) mark the locations of digital images presented in figure 12, which alternate between stable and unstable configurations depending on the route taken through the parameter space. All images are for an identical value of Q and increasing values of U.

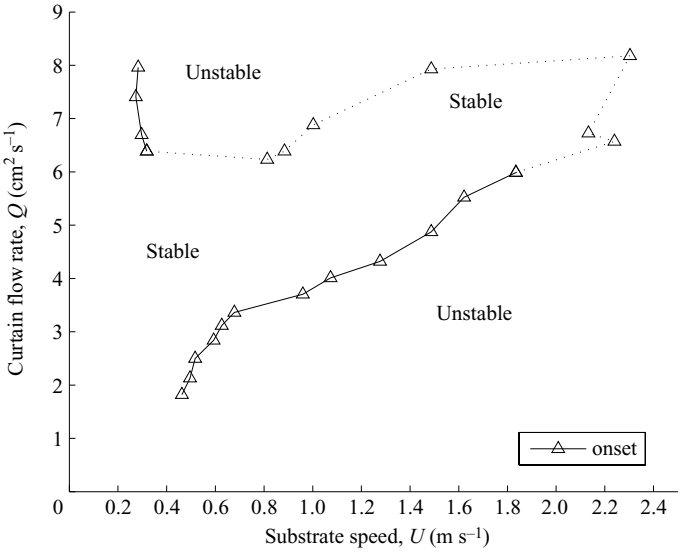

FIGURE 10. Stability/instability curve for the 0.597 Pa s solution (original onset data points from figure 7 (solid line) with additional points (dotted line) created by alternately increasing both curtain flow rate and substrate speed to keep inside the stable region). The stable region within the dotted line is the extra region of stability obtained by varying the path through the Q–U space. For $6.2\,\mathrm{cm^2\,s^{-1}} < Q < 8\,\mathrm{cm^2\,s^{-1}}$ the speed for the onset of air entrainment is not unique. $2.39 < Ca < 21.2$, $0.386 < Re < 1.73$.

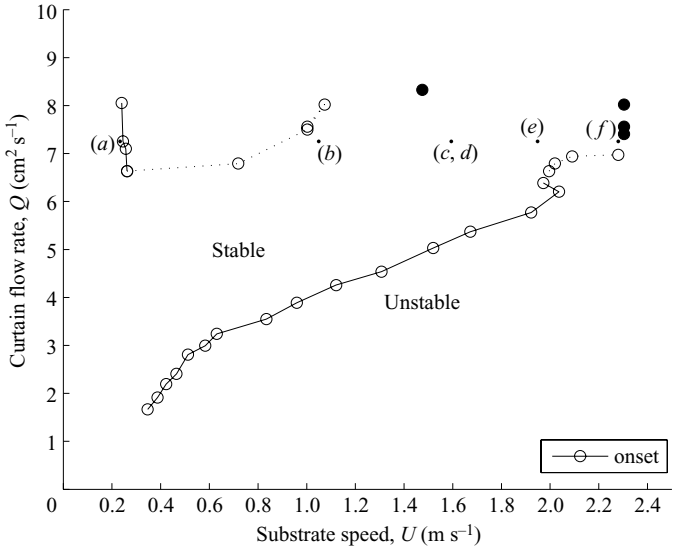

FIGURE 11. Stability/instability curve for a 0.608 Pa s solution ($\sigma = 0.0665\,\mathrm{N\,m^{-1}}$). Upper and lower onset branches (solid lines) with additional points (dotted lines) created using the method described in § 3.3. The filled circles represent the limitations of the equipment, hence a closed stable region could not be found for this fluid. For $Q > 6.38\,\mathrm{cm^2\,s^{-1}}$ the speed for the onset of air entrainment is not unique. The letters indicate the locations of the digital images of the contact line presented in figure 12. $2.19 < Ca < 21.03$, $0.35 < Re < 1.73$.

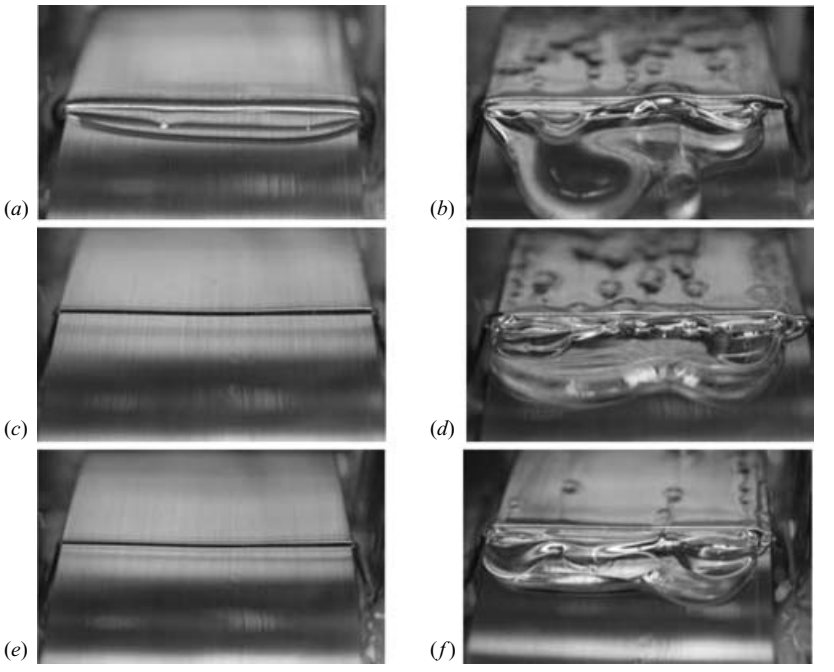

FIGURE 12. Digital photographs corresponding to the locations marked on the air entrainment curve in figure 11. All images are for $Q = 7.25\,\mathrm{cm^2\,s^{-1}}$. $U = 0.23, 1.05, 1.59, 1.59, 1.95, 2.28\,\mathrm{m\,s^{-1}}$ for (a)–(f) respectively. The flow parameters were reached using various paths to produce either stable or unstable configurations. Images (c) and (d) are for identical parameters. Images are taken from the rear of the curtain.

In comparison, figure 13 shows data points from both a horizontal and path-dependent analysis which form a closed region of stability.

In figures 10, 11, 12 and 13, it has been seen that two different flows may occur for identical parameter values, depending on the route taken through the parameter space. Therefore, there are, in some sense, two attracting solutions available at certain points in the Q–U parameter space. At certain points in the Q–U plane, the flow is only stable if the route through the Q–U space is entirely via the stable domain.

4. Conclusions

The stability of the contact line in curtain coating has been observed experimentally for both low- and high-viscosity fluids in the case where the substrate is pre-wetted with a thin film of the coating fluid. It has been shown that for higher viscosity liquids, altering the path taken through the Q–U parameter space to arrive at the onset of instability may give two distinct speeds at which the contact line becomes unstable.

The observation of two speeds for the onset of instability was only found by a path-dependent analysis, at substantially higher flow rates. Furthermore, only one critical speed for the re-emergence of stability was identified here, hence these observations are qualitatively different from previous studies.

The observations of path-dependent instability made for the higher viscosity fluid appear to be exclusive to the situation of 'intense' hydrodynamic assist. In comparison, it is unclear whether the hysteresis identified in figures 3, 5 and 7 between the onset and clearance boundaries is the same phenomenon, since here

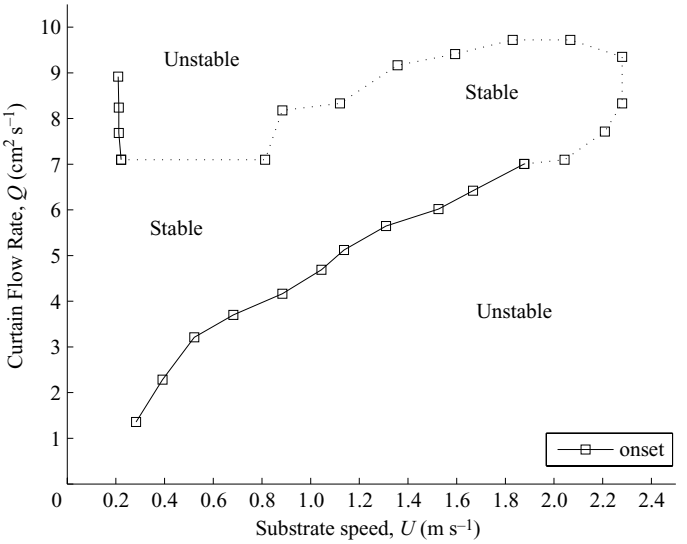

FIGURE 13. Stability/instability curve for a 0.498 Pa s solution ($\rho = 1264\,\mathrm{kg\,m^{-3}}$, $\sigma = 0.0652\,\mathrm{N\,m^{-1}}$) created using the method described in § 3.3. The data points joined by the dotted line define the extra region of stability obtained by varying the path through the Q–U space. For $7.1\,\mathrm{cm^2\,s^{-1}} < Q < 9.7\,\mathrm{cm^2\,s^{-1}}$ the speed for the onset of air entrainment is not unique. $1.6 < Ca < 17.41$, $0.34 < Re < 2.46$.

onset and clearance of instability might occur at different speeds due to entrained air remaining in the film onto which coating occurs. In these hysteresis observations arising from clearance, the coating speed is decreased after instability as the clearance boundary is approached, which is quite different from the path-dependent stability boundaries seen in figures 10, 11 and 13.

Correlation of air entrainment data usually involves inverse power laws; however, the data presented here suggest that for matching impingement speeds and flow rates, the coating speed can increase with viscosity. This contradiction with previous correlations is due to a combination of intense hydrodynamic assist, favoured by a high liquid viscosity, and the lubrication effect of the residual film on the surface.

In summary, the idea of stable coating for speeds below some critical substrate speed for a fixed flow rate, with instability occurring at speeds above this critical speed, needs to be re-examined, at least for coating onto a pre-wetted surface, since there are, in some cases, more than two critical speeds. Since multiple stable regions have been identified for dry substrates (Clarke 2002; Blake *et al.* 2004), we postulate that the observations of path-dependent stability boundaries may also occur for dry wetting, since the method described in § 3.1 is the usual experimental one for dry wetting too, as opposed to that used in § 3.3.

Determining a maximum speed of coating for a given flow rate is commercially desirable. However, the results here suggest that this speed may, in some cases, be significantly higher than the speed at which air entrainment first occurs when increasing the substrate speed for a fixed flow rate.

The authors would like to thank Tom Carpenter and Paul Shearing for collection of data in figure 13 and Kenneth Lee for taking digital images. Their work is greatly appreciated.

REFERENCES

Benkreira, H. 2002 Experimental study of dynamic wetting in reverse-roll coating. *AIChE J.* **48**, 221–226.

Benkreira, H. 2004 The effect of substrate roughness on air entrainment in dip coating. *Chem. Engng Sci.* **59**, 2745–2751.

Blake, T. D. 2005 The physics of moving wetting lines. *Proc. 6th European Coating Symposium, Bradford*.

Blake, T. D., Bracke, M. & Shikhmurzaev, Y. D. 1999 Experimental evidence of nonlocal hydrodynamic influence on the dynamic contact angle. *Phys. Fluids* **11**, 1995–2007.

Blake, T. D., Clarke, A. & Ruschak, K. J. 1994 Hydrodynamic assist of dynamic wetting. *AIChE J.* **40**, 229–242.

Blake, T. D., Dobson, R. A. & Ruschak, K. J. 2004 Wetting at high capillary numbers. *J. Colloid Interface Sci.* **279**, 198–205.

Blake, T. D. & Ruschak, K. J. 1979 A maximum speed of wetting. *Nature* **282**, 489–491.

Blake, T. D. & Shikhmurzaev, Y. D. 2002 Dynamic wetting by liquids of different viscosity. *J. Colloid Interface Sci.* **253**, 196–202.

Burley, R. & Jolly, R. P. S. 1984 Entrainment of air into liquids by a high speed continuous solid surface. *Chem. Engng Sci.* **39**, 1357–1372.

Burley, R. & Kennedy, S. B. 1976 An experimental study of air entrainment at a solid/liquid/gas interface. *Chem. Engng Sci.* **31**, 901–911.

Chen, X., Rame, E. & Garoff, S. 2004 The effects of thin and ultrathin liquid films on dynamic wetting. *Phys. Fluids* **16**, 287–297.

Clarke, A. 2002 Coating on a rough surface. *AIChE J.* **48**, 2149–2156.

Cohu, O. & Benkreira, H. 1998 Air Entrainment in angled dip coating. *Chem. Engng Sci.* **53**, 533–540.

Ghannam, M. T. & Esmail, M. N. 1993 Experimental study of the wetting of fibres. *AIChE J.* **39**, 361–365.

Gutoff, E. B. & Kendrick, C. E. 1982 Dynamic contact angles. *AIChE J.* **28**, 459–466.

Lin, S. P. & Roberts, G. 1981 Waves in a viscous liquid curtain. *J. Fluid Mech.* **112**, 443–458.

Miyamoto, K. & Katagiri, Y. 1997 Curtain coating. In *Liquid Film Coating* (ed. S. F. Kistler & P. M. Schweizer). Chapman & Hall.

Weinstein, S. J. & Ruschak, K. J. 2004 Coating flows. *Annu. Rev Fluid Mech.* **36**, 29–53.